

Short Communication

Investigation of Multilayer Brazed Aluminium Corrosion Process by Electrochemical Noise

Longjun Guo^{1,2}, Jihui Wang^{1,2,*}, Wenbin Hu^{1,3}

¹ Tianjin Key Laboratory of composite & Functional Materials, School of Materials Science and Engineering, Tianjin University, Tianjin, 300072, China.

² State Key Laboratory of Hydraulic Engineering Simulation and Safety, Tianjin University, Tianjin 300072, P R China.

³ Key Laboratory of Advanced ceramics and Machining Technology (Ministry of Education), Tianjin Univ. Tianjin, 300072, China.

*E-mail: jhwang@tju.edu.cn

Received: 1 December 2017 / Accepted: 4 January 2018 / Published: 5 February 2018

The corrosion process of a multilayer aluminum brazed sheet AA4045/AA3003*/AA4045 in EXCO solution was investigated by electrochemical noise (EN) technique. Cluster analysis and discrete wavelet transform analysis were performed to investigate EN data. Results showed that the corrosion process can be identified by cluster analysis and the energy distribution plot (EDP) extracted from EN data. As immersion time increased, the corrosion process of the multilayer brazed sheet changed from pitting corrosion (PC) to inter-granular corrosion (IGC) to exfoliation corrosion (EC), and then back to IGC. The maximum relative energy in EDP changed from small scale to middle scale to large scale and then back to middle scale. This finding shows a good agreement with the cluster analysis result. By coupled with the EN technique and corrosion morphology, EDP and cluster analysis can be used to study the corrosion process of multilayer brazed sheet.

Keywords: Multilayer aluminum, electrochemical noise, cluster analysis, wavelet transformation, corrosion process

1. INTRODUCTION

Aluminum brazed sheet has been widely used in the field of automotive heat exchangers, such as in air conditioners, evaporators, radiators, and engine cooling systems, because of their low density, favorable thermal conductivity, satisfactory mechanical properties, and relatively good corrosion resistance [1-3]. In an actual environment, however, exhaust gases will flow repeatedly through a heat exchanger. When mixed with water vapor, these exhaust gases will form strong acids, such as nitric

acid (HNO_3), hydrochloric acid (HCl), sulfuric acid (H_2SO_4), and organic acids [4]. These acids will cause aluminum brazed sheets to easily develop localized corrosion, such as pitting corrosion (PC), inter-granular corrosion (IGC), and exfoliation corrosion (EC) when subjected to aggressive environments, which can eventually lead to engine breakdown due to overheating. In such case, the corrosion problem of aluminum brazed sheet becomes a concern.

Several ex-situ electrochemical techniques (e.g., open circuit potential, cyclic voltammetry, and potentiodynamic polarization [5-8]), and the non-electrochemical techniques (e.g., immersion test, seawater acidified accelerated test, copper accelerated salt spray test, and acetic acid salt spray test [7, 9, 10]) have been used to research the corrosion behavior of aluminum brazed sheet. However, the aforementioned ex-situ electrochemical techniques are typically conducted under external input electrical signals, which may disturb the experimental system. Meanwhile, non-electrochemical techniques may be time-consuming. Furthermore, previous studies have mainly focused on the corrosion properties of the microstructure of aluminum brazed sheet. Only a few studies have been performed on the corrosion propagation process of a aluminum brazed sheet by electrochemical noise (EN) technique.

The current study aimed to explore the corrosion propagation process of a multilayer brazed sheet in EXCO solution by using the EN technique. A typical system, i.e., an AA4045/AA3003*/AA4045 multilayer brazed sheet in EXCO solution, was selected, and long-term continuous EN time records were applied to the analysis.

2. EXPERIMENTAL

2.1. Materials and solutions

The multilayer brazed sheet is composed a modified AA3003* aluminum alloy (190 μm thick) clad on both sides with an AA4045 aluminum alloy (20 μm thick). The chemical composition of the core material (AA3003*) is listed as follows: 0.10 wt.% Si, 0.12 wt.% Fe, 0.65 wt.% Cu, 1.60 wt.% Mn, 0.02 wt.% Mg, 0.10 wt.% Ti and balanced Al; and the clad layer material (AA4045) is listed as follows: 10 wt.% Si, 0.45 wt.% Fe, 0.10 wt.% Cu, 0.02 wt.% Mg and balanced Al. The accelerated corrosion test was carried out in EXCO solution (4 M NaCl, 0.5 M KNO_3 , 0.1 M HNO_3 (70 wt.%) and 1 L H_2O) for 96 h at 25 °C in accordance with the EXCO test standard of ASTM G34-79.

2.2. Electrochemical noise measurement

The EN measurement was carried out by a CST500 electrochemical workstation. The scheme of the electrochemical cell is shown in Fig.1. A pair of nominally identical brazed sheet was used as working electrode (WE) and the reference electrode (RE) was a saturated calomel electrode (SCE) with a Luggin capillary. The exposed area of the working electrode was 1 cm^2 . The potential and current noise were recorded simultaneously for 96 hours at a sampling frequency of 2 Hz, within a period of 512 s for each record.

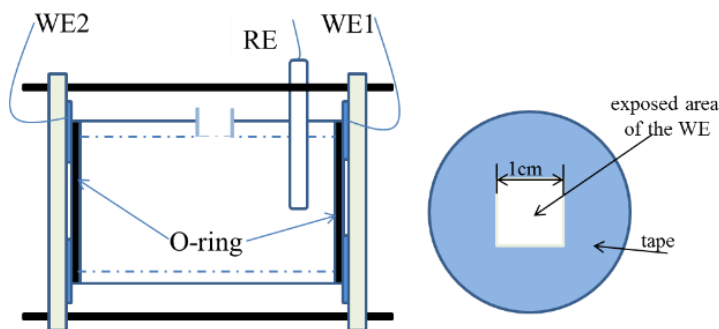


Figure 1. Scheme of the electrochemical cell.

2.3. Electrochemical noise analysis

2.3.1. Cluster analysis

Cluster analysis (CA) is a widely used technique in the area of pattern recognition. It is a classification tool to find teams of datasets with similar characteristics. It is suitable to apply K -means cluster analysis, when the datasets of the EN is larger than 100 [11]. The algorithm of this method consists of two steps: firstly, compute the distances from each individual data point to the center of each cluster centroid using the pooled-within covariance matrix; secondly, assign each point to the cluster to which it is closest. In the above two steps, the distances measure and cluster formation are achieved through squared Euclidean distance measure and Ward's method, respectively [12]. The expression of gravitational center and squared Euclidean distance of each cluster (D_k^2) can be expressed as follows:

$$\bar{x}_{jk} = \frac{1}{m_k} \sum_{i=1}^{m_k} x_{ijk}$$

$$D_k^2 = \sum_{j=1}^n \sum_{i=1}^{m_k} (x_{ijk} - \bar{x}_{jk})^2$$

Where x_{ijk} is the variable j of case i in cluster k , \bar{x}_{jk} is the center of the cluster k and m_k is the number of the cases in cluster k .

Finally, variance (ANOVA) analysis is performed to verify the separation of the clusters within each one. Good separation will be proven when the significance is nearer to zero ($P \ll 0.001$).

Statistical parameters such as noise resistance (R_n) [13,14], standard deviation (σ_v and σ_i) [15-17], wavelet dimension (D_v and D_i) [18-20], average charge (q) [14,21,22], and frequency of events (f_n) [14,21,22] have been widely used in EN data analysis. In this work, all of these statistics (675 groups) were selected for cluster analysis of EN data by using SPSS 22 software.

2.3.2. Wavelet analysis

The measured EN data was analyzed with wavelet transform using the MATLAB R2014a software. Although the electrochemical noise technique allows the acquisition of both signals (E and I), but only the current noise was analyzed [23]. This is because potential transients reflect capacitive discharge process, while current transients reflect initiation, growth, and repassivation processes [23].

Therefore, we only use the current noise data to analysis the corrosion process. The electrochemical current noise (ECN) was performed using an orthogonal db4 wavelet, with seven levels (d_1 - d_7 , a_7) of decomposition. Time scale of each detailed crystal after wavelet decomposition in the case of 2 Hz sampling frequency was listed in Table 1. To represent wavelet transformation in more details, the energy distribution plot (EDP), as a relative energy of a crystal, was plotted versus the crystal name. The data process was detailed described in Refs. [24-26].

The overall detail energy E of the signal was calculated as follows:

$$E = \sum_{n=1}^{N/2} d_{1,n}^2 + \sum_{n=1}^{N/2^2} d_{2,n}^2 + \dots + \sum_{n=1}^{N/2^7} d_{7,n}^2$$

The each detail crystal (E_j^d) was calculated as follows:

$$E_j^d = \frac{1}{E} \sum_{n=1}^{N/2^j} d_{j,n}^2 \quad (j = 1, 2, \dots, 7)$$

Table 1. Frequency and time scale of each detailed crystal for $j = 7$ and $f_s = 2$ Hz.

Crystal	Frequency range / Hz	Time scale / s
d_1	2~1	0.5~1
d_2	1~0.5	1~2
d_3	0.5~0.25	2~4
d_4	0.25~0.125	4~8
d_5	0.125~0.0625	8~16
d_6	0.0625~0.03125	16~32
d_7	0.03125~0.015625	32~64

3. RESULTS

3.1. Microstructure

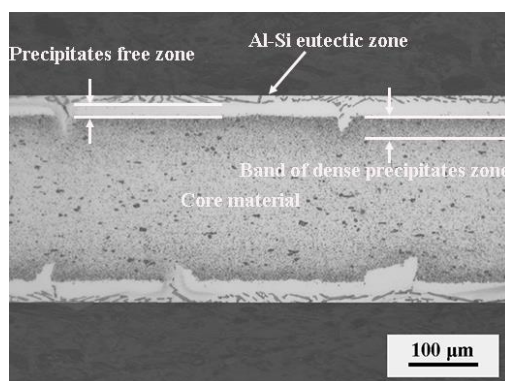


Figure 2. Cross-section micrograph of the brazed multilayer aluminum sheet.

Fig. 2 shows the cross-section micrograph of the brazed multilayer aluminum sheet. The first layer was the Al-Si eutectic zone, which mainly consisted of needlelike silicon and eutectic α -Al. The second layer was the precipitate-free zone (PFZ), which mainly comprised elongated coarse primary α -

Al grains. The third layer was the band of dense precipitate zone (BDP), which was mainly composed of a large number of α -Al(Mn,Fe)Si particles and measured approximately 40 μm . The fourth layer was the core material, which contained an uneven distribution of dark particles.

3.2. Observation of corroded morphologies

The surface and cross-section morphologies of the brazed sheets after 3, 24, 48, and 96 h of immersion in EXCO solution are depicted in Figs. 3 and 4, respectively. After 3 h, several pits were observed on the surface (Fig. 3a) and cross-section (Fig. 4a) images. These pits were due to the dissolution of eutectic α -Al grains, which were surrounded by cathodic particles, such as Al_2Cu and α -Al(Mn,Fe)Si particles. This IGC attack is observed on the surface (Fig. 3b) and cross-section (Fig. 4b) images. After 48 h of immersion test, an IGC attack developed in the BDP zone in the form of EC (Figs. 3c and 4c). After 96 h of immersion in EXCO solution, the BDP zone was peeled off and the core material was attacked by IGC (Figs. 3d and 4d).

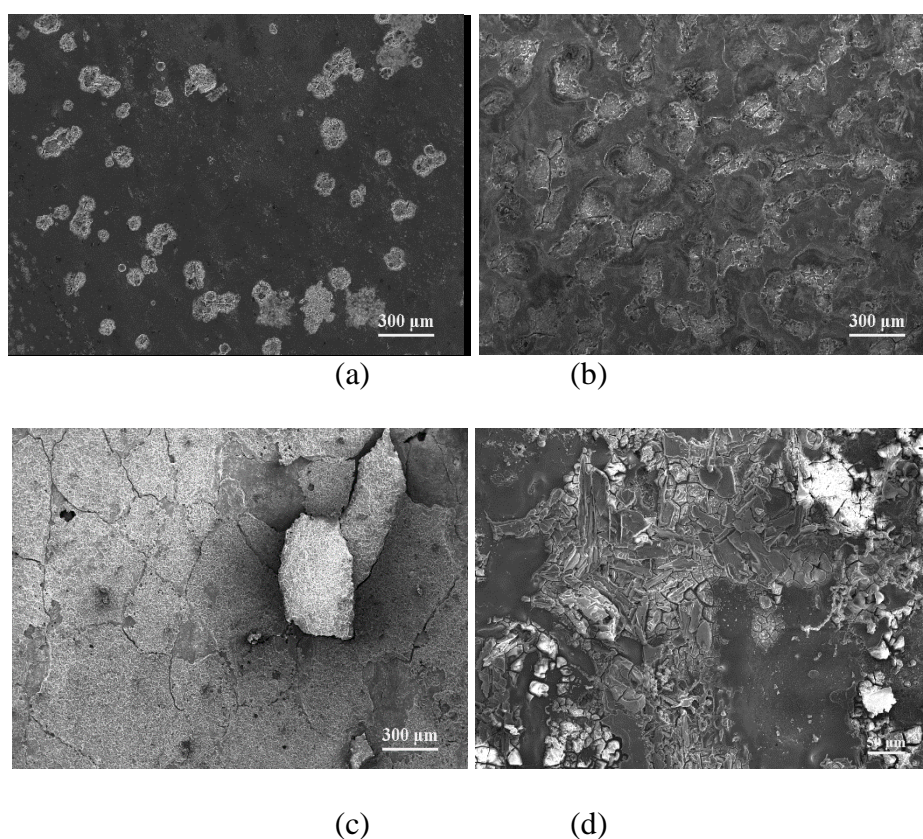


Figure 3. Surface morphologies of the brazed sheets after immersion in EXCO solution: (a) 3 h, (b) 24 h, (c) 48 h, (d) 96 h.

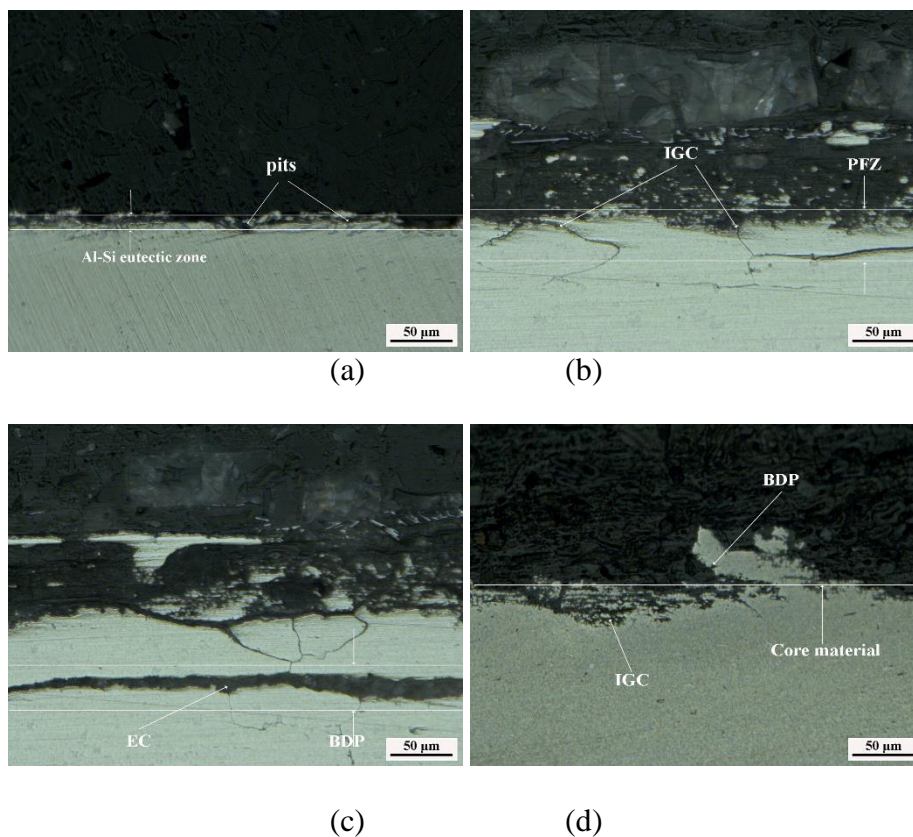


Figure 4. Cross-section morphologies of the brazed sheets after immersion in EXCO solution: (a) 3 h, (b) 24 h, (c) 48 h, (d) 96 h.

3.3. EN characterization

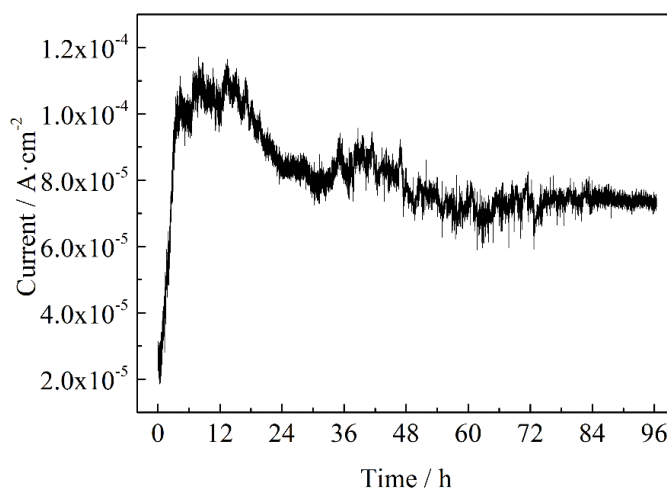


Figure 5. ECN record of the brazed sheet during 96 h of immersion in EXCO solution.

The electrochemical current noise (ECN) of the brazed sheet during 96 h of immersion in EXCO solution is shown in Fig. 5. A direct current trend was observed in current noise. The current abruptly and then slowly increased before 24 h, and then decreased thereafter. These phenomena

indicated that an increase in the cathodic reaction rate was predominant, and then the decrease of the anodic reaction rate became the dominant factor. This situation was probably due to a change in the surface oxide layer [27,28].

3.3.1 Cluster analysis

The parameters extracted from EN data during 96 h measurement are shown in Fig. 6. The result indicates that determining the corrosion process based on only one or several parameters is inaccurate. Therefore, all the parameters (675 groups) are selected for the *K*-means cluster analysis of EN data to achieve an objective evaluation of the corrosion process. The cluster number was set to 3, i.e., Clusters 1, 2, 3, which corresponded to PC, IGC, EC, respectively. Fig. 7 and Table 2 show the cluster results of the brazed sheet during 96 h of immersion in EXCO solution. At stage I (0-16 h), the data belong to Cluster 1. At stage II (16-28 h), the data overlap in the two clusters at the beginning (i.e., 11% of the data are in Cluster 1 and the remaining data are in Cluster 2), which indicates a transitional stage between Clusters 1 and 2. At stage III (28-72 h), the data overlap in two clusters (i.e., 49% of the data are in Cluster 2 and the remaining data are in Cluster 3), which indicates that Clusters 2 and 3 occur simultaneously during this stage. At stage IV (72-96 h), the data belong to Cluster 2. Table 3 shows the ANOVA results of the cluster analysis, which confirm the validity of the cluster analysis ($P \ll 0.001$).

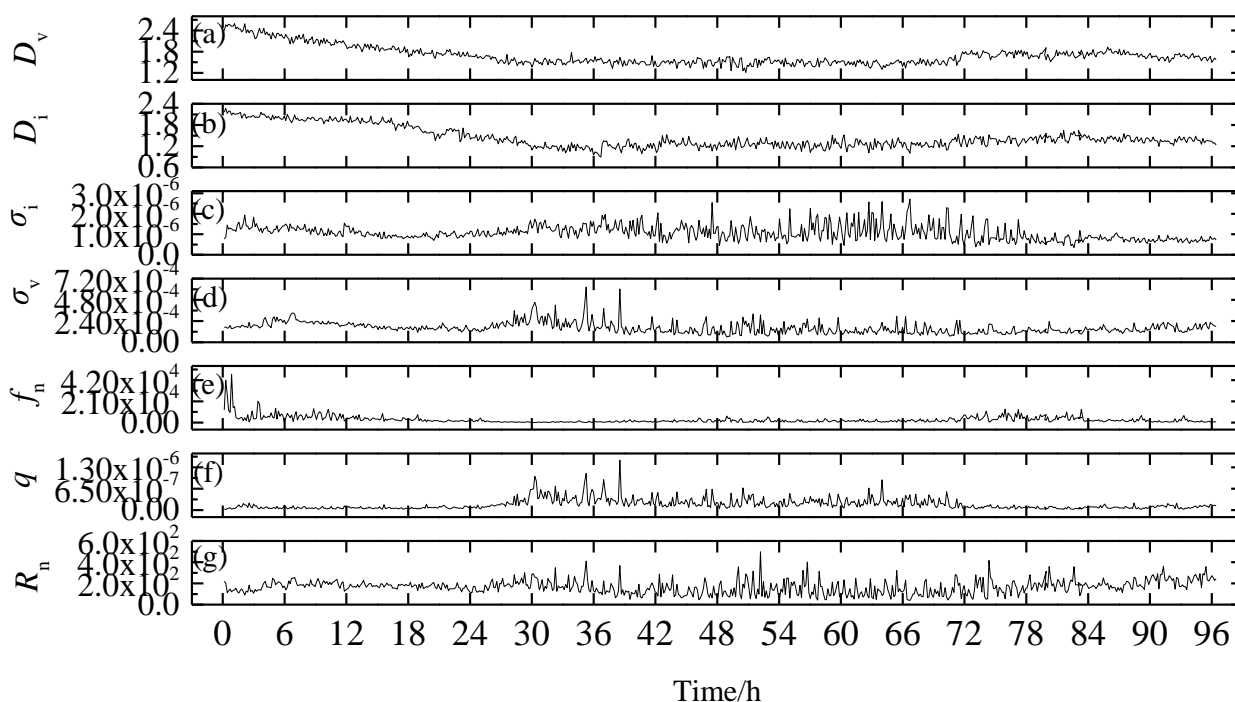


Figure 6. Parameters extracted from EN data during 96 h measurement: (a) wavelet potential dimension D_v , (b) wavelet current dimension D_i , (c) current standard deviation σ_i , (d) potential standard deviation σ_v , (e) frequency of events f_n , (f) average charge q and (g) noise resistance R_n .

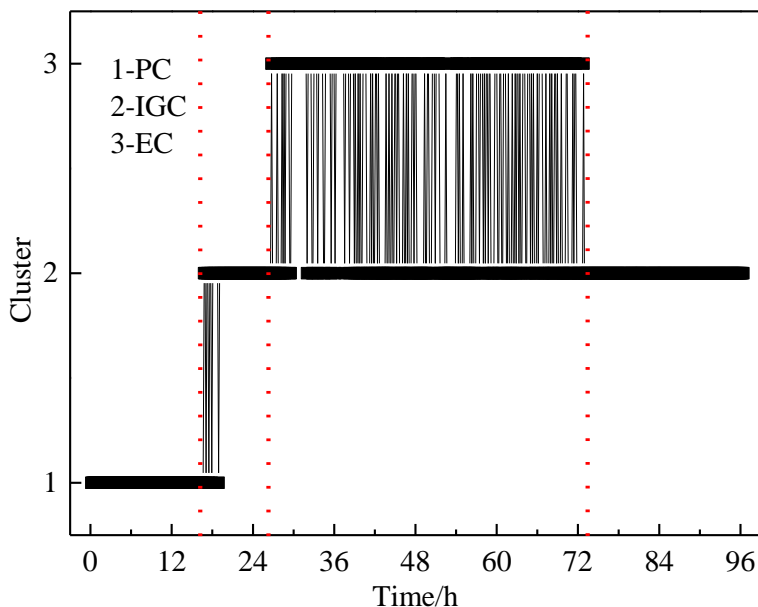


Figure 7. Cluster distribution as the function of time for the brazed sheet immersion in EXCO solution for 96 h.

Table 2. Cluster results of EN data of the brazed sheet during 96 h of immersion in EXCO solution.

Stage	Time period	Total Number	Number/Percentage			Corrosion type
			Cluster1	Cluster2	Cluster3	
I	0-16.07 h	112	112/100%	0	0	PC
II	16.21-28.01 h	83	9/11%	74/ 89%	0/0	IGC
III	28.16-72.96 h	311	0	154/49%	157/51%	IGC&EC
IV	72.11-96 h	169	0	169/100%	0	IGC

Table 3. Univariate analysis of variance for the cluster analysis of EN data.

	Cluster		Error		F	Significance
	Mean square	d.f.	Mean square	d.f.		
σ_v	79.700	2	0.767	675	103.936	P<0.001
q	204.229	2	0.398	675	513.343	P<0.001
σ_i	167.816	2	0.506	675	331.827	P<0.001
R_n	10.284	2	0.972	675	10.575	P<0.001
f_n	86.484	2	0.747	675	115.820	P<0.001
D_i	280.327	2	0.172	675	1626.375	P<0.001
D_v	244.109	2	0.280	675	872.827	P<0.001

3.3.2 Wavelet analysis

Fig. 8 shows the decomposed results of ECN. The origin current signal s is displayed at the top. The crystals d_1 to d_7 denote the details of the origin signal, and a_7 denotes the approximation part of

the origin signal. The decomposed results indicated that the detail crystals of the origin signal changed with immersion time.

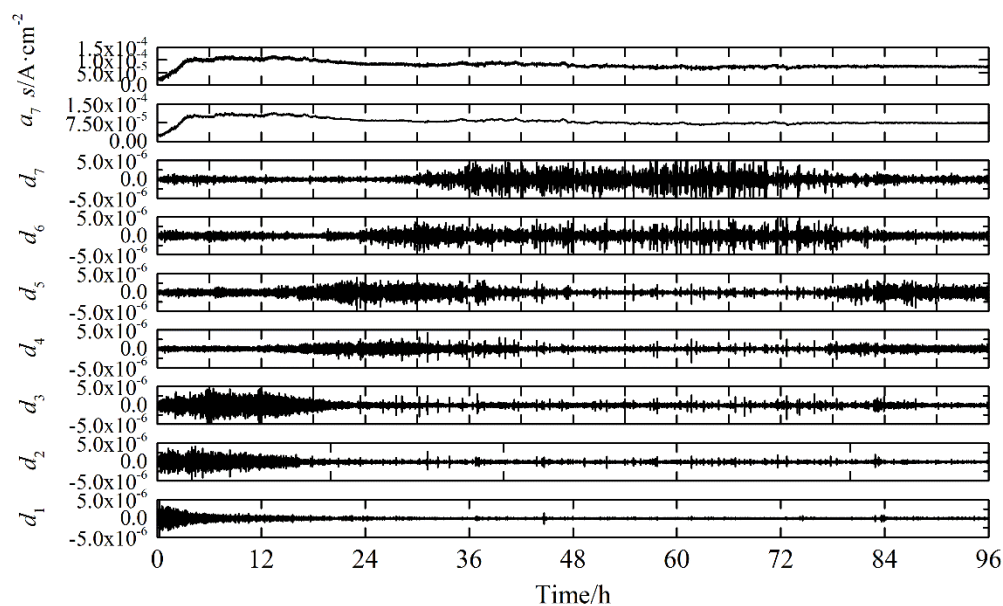


Figure 8. Seven-level wavelet decomposition with a Daubechies 4 wavelet of ECN in Figure. 5.

The ECN signals of the brazed sheets after 3, 24, 48, and 96 h of immersion in EXCO solution are depicted in Fig. 9. The direct current trend of EN data was removed by using a 5-order polynomial fitting.

Fig. 9a shows the ECN signals at 3 h. The duration of the current transient was several seconds (3 s in the insert plot). Fig. 9b shows that the maximum relative energy is within the small scale range in the EDPs, and the electrode surface is under PC attack as illustrated in the corresponding images of the corroded surface (Figs. 3a and 4a).

Fig. 9c shows the ECN signals at 24 h. The duration of the current transient was ten seconds (12 s in the insert plot). Fig. 9d shows that the maximum relative energy is in the position of middle scale d_5 in the EDPs, and the main corrosion type is IGC, which is proven by the corresponding corroded surface (Figs. 3b and 4b).

Fig. 9e shows the ECN signals at 48 h. The duration of the current transient was several ten seconds (45 s in the insert plot). Fig. 9f shows that the maximum relative energy is in the position of large scale d_7 in the EDPs. The main electrode surface is EC (Figs. 3c and 4c).

Fig. 9g shows the ECN signals at 96 h. The duration of the potential transient was 13 s, as illustrated in the insert plot. Fig. 9h shows that the maximum relative energy is in the position of middle scale d_5 in the EDPs. The main corrosion type on the surface is IGC (Figs. 3d and 4d).

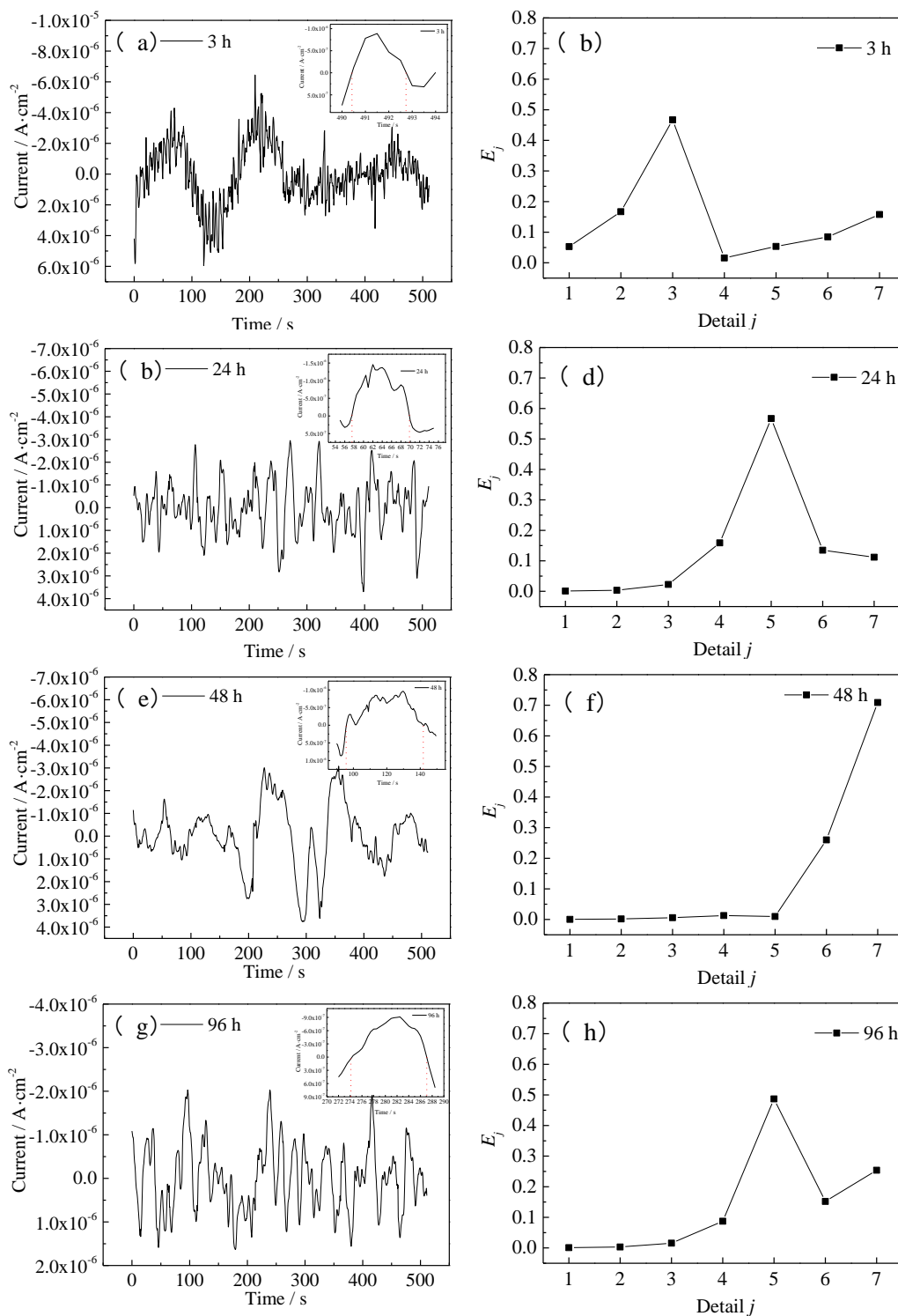


Figure 9. The brazed sheet after 3, 24, 48, and 96 h of immersion in EXCO solution: a, c, e, g) the ECN signals, remove the dc trend; b, d, f, h) the corresponding EDP.

Fig. 10 shows the evolution of the EDPs of the brazed sheet during 96 h of immersion in EXCO solution. Based on the above results, four corrosion stages were believed to occur. At Stages I, II, III, and IV, the maximum relative energy mainly accumulated at the positions of small scale d_3 , middle scale d_5 , large scale d_7 , and middle scale d_5 , respectively.

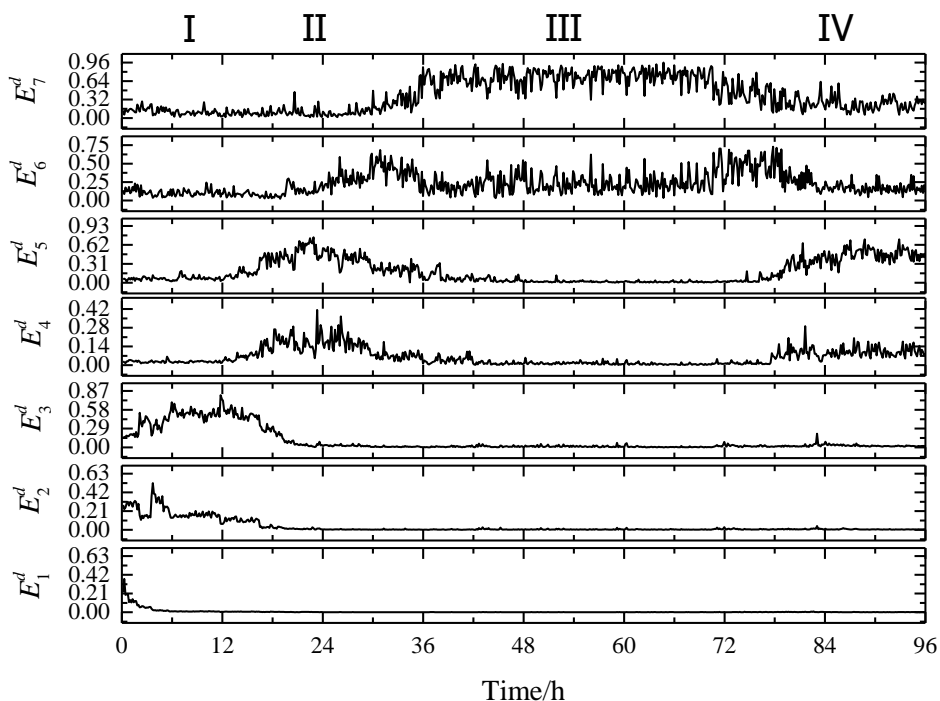


Figure 10. Evolution of EDPs (E_j^d) as the function of time for the brazed sheet immersion in EXCO solution for 96 h.

4. DISCUSSION

During the initial 16 h of immersion of the aluminum brazed sheet in EXCO solution, the first layer of the brazed sheet was in contact with the corrosive solution, and would be corroded first. Fig. 2 shows several intermetallic precipitates, such as Al_2Cu and $\alpha\text{-Al}(\text{Mn,Fe})\text{Si}$ particles, in the eutectic $\alpha\text{-Al}$ grains of the first layer. Several studies have shown that the corrosion potential of these intermetallic particles is nobler than that of the aluminum matrix [29, 30], which induces many microgalvanic cells to form localized corrosion. Consequently, eutectic $\alpha\text{-Al}$ can be attacked first by PC (Figs. 3a and 4a). In general, the nucleation and growth of PC always occur prior to other localized corrosion, and are significantly faster than aggressive ions diffusion and corrosion products desorption [31]. Some studies have shown that transients related to PC have a lifetime higher than 2 s [23]. Therefore, the maximum relative energy is within the small scale range in the EDPs (Fig. 9b), which reveals that a PC attack is occurring at the electrode surface. Furthermore, the remarkable maximum relative energy at d_3 shows that metastable pits are propagating and developing into stable pits, as illustrated in Fig. 3b.

PC propagates in width and depth toward the second layer of the brazed sheet with immersion time, which causes the second layer to come in contact with the corrosive solution. The second layer is PFZ (Fig. 2). This layer consists of primary $\alpha\text{-Al}$ grains and several intermetallic particles in the primary $\alpha\text{-Al}$ grain boundaries [8,9,32]. These intermetallic particles are expected to form galvanic cells. At this time, the duration of the current transient is longer than the current transient before 16 h,

and the maximum relative energy occurs at the position of d_5 in the EDPs, thereby suggesting that the grain boundaries of the primary α -Al is under IGC attack (Figs. 3b and 4b).

As immersion reached 48 h, the corrosion attack moved along the primary α -Al grain boundaries toward the third layer (i.e., the BDP zone shown in Fig. 2). The reduction of manganese and copper in the BDP zone results in a lower corrosion potential [1, 33, 34] which makes this zone more prone to corrosion than the inner core structure. During this stage, the duration of the current transient reached 40 s (Fig. 9g), which indicates that the corrosion process occurred slowly in the electrode surface. This finding is attributed to the accumulation of corrosion products between the BDP zone and the core material interface, which hinders oxygen diffusion from the solution to the interface, and the opposite diffusion of several intermediate corrosion products. Furthermore, the conglomeration of hydrogen bubbles and corrosion products at the interface will lead to wedge-shaped stress, thereby causing the upper grains of the BDP zone to peel off the inner grains of the core material. Thus, the negatively drifted transient will take longer to restore to the background compared with other localized corrosion types, such as PC and IGC [31,32]. Consequently, the maximum relative energy occurs at the largest crystal d_7 in the EDPs (Figs. 9f and 10).

As the immersion time increases on 96 h, the BDP zone was peeled off, and the core material was attacked by IGC. Several studies show have reported the presence of Al_2Cu particles in the grain boundaries of the core material [7,35,32]. This condition is assumed as one of the main reasons for the development of IGC in the core structure of the brazed sheet. Meanwhile, the maximum relative energy returns to the middle crystal d_5 in the EDPs (Figs. 9h and 10).

From the preceding discussion, cluster analysis and EDP extracted from EN data can be used to differentiate the corrosion propagation process of a multilayer AA4045/AA3003*/AA4045 aluminum brazed sheet.

5. CONCLUSIONS

(1) The corrosion process of a multilayer aluminum brazed sheet in EXCO solution can be divided into four stages using K -means cluster analysis.

(2) As the corrosion process of the multilayer aluminum brazed sheet changes in EXCO solution, the maximum relative energy in EDP will change from small scale to middle scale to large scale, and then back to middle scale.

ACKNOWLEDGEMENTS

This paper was jointly supported by National Basic Research Program of China (2014CB046801), National Natural Science Foundation of China (51471117) and Key Project of Tianjin Natural Science Foundation (13JCZDJC29500).

References

1. J. Lacaze, S. Tierce, M.C. Lafont, Y. Thebault, N. Pébère, G. Mankowski, C. Blanc, H. Robidou, D. Vaumousse and D. Daloz, *Mater. Sci. Eng. A*, 413 (2005) 317.

2. C.A. Tadgell, M.A. Wells, S.F. Corbin, L. Colley, B. Cheadle and S. Winkler, *Met. Trans. A*, 48 (2017) 1236.
3. M.J. Benoit, M.A. Whitney, M.A. Wells and S. Winkler, *Met. Trans. B*, 47 (2016) 3501.
4. S. Iwao, M. Yoshino, M. Edo and S. Kuroda, *Corrosion*, 71 (2015) 598.
5. F.M. Al-Kharafi, W.A. Badawy, *Electrochim. Acta*, 40 (1995) 1811.
6. S.S. Abdel Rehim, H.H. Hassan and M.A. Amin, *Corros. Sci.*, 46 (2004) 1921.
7. F.N. Afshar, J.H.W. de Wit, H. Terryn and J.M.C. Mol, *Electrochim. Acta*, 88 (2013) 330.
8. F.N. Afshar, R. Ambat, C. Kwakernaak, J.H.W. de Wit, J.M.C. Mol and H. Terryn, *Electrochim. Acta*, 77 (2012) 285.
9. F.N. Afshar, A.M. Glenn, J.H.W. de Wit, H. Terryn and J.M.C. Mol, *Electrochim. Acta*, 104 (2013) 48.
10. S. Tierce, N. Pébère, C. Blanc, C. Casenave, G. Mankowski and H. Robidou, *Electrochim. Acta*, 52 (2006) 1092.
11. J.Y. Huang, Y.B. Qiu and X.P. Guo, *Electrochim. Acta*, 54 (2009) 2218.
12. J.Y. Huang, X.P. Guo, Y.B. Qiu and Z.Y. Chen, *Electrochim. Acta*, 53 (2007) 680.
13. C. Gouveia-Caridade, M. Pereira and C. Brett, *Electrochim. Acta*, 49 (2004) 785.
14. A. Mandujano-Ruíz, J. Morales-Hernández, F. Castañeda-Saldivar, H. Herrera-Hernández and J.M. Juárez-García, *Int. J. Electrochem. Sci.*, 13 (2018) 1062.
15. J.X. Su, Z. Zhang, Y.Y. Shi, F.H. Cao and J.Q. Zhang, *Mater. Corros.*, 57(2006) 484.
16. C. Ma, S.Z. Song, Z.M. Gao, J.H. Wang and W.B. Hu, *Corros. Eng. Sci. Techn.*, 52 (2017) 432.
17. D.H. Xia, C. Ma, S.Z. Song, L.L. Ma, J.H. Wang, Z.M. Gao, C. Zhong and W.B. Hu, *Sens. Actuat. B Chem.*, 252 (2017) 353.
18. J.J. Kim, *Met. Mater. Int.*, 17 (2011) 777-782.
19. J.J. Kim, *Mater. Lett.*, 61 (2007) 4000-4002.
20. D.H. Xia, S.Z. Song and Y. Behnamian, *Corros. Eng. Sci. Techn.*, 51 (2016) 527.
21. J.M. Sanchez-Amaya, R.A. Cottis, F.J. Botana, *Corros. Sci.*, 47 (2005) 3280.
22. J.M. Sánchez-Amaya, M. Bethencourt, L. González-Rovira and F.J. Botana, *Electrochim. Acta*, 52 (2007) 6569.
23. E. Rios, A. Zimer, P. Mendes, M. Freitas, E. de Castro, L. Mascaro and E. Pereira, *Fuel*, 150 (2015) 325.
24. A. Aballe, M. Bethencourt, F.J. Botana and M. Marcos, *Electrochim. Acta*, 44 (1999) 4805.
25. Y. Yang, Y. Chen, X.Q. Du, S. Feng and Z. Zhang, *Int. J. Electrochem. Sci.*, 13 (2018) 384.
26. Y. Zhao, X. Wang, F. Li, R.W. Zhang, J.C. Huang and M. Wu, *Int. J. Electrochem. Sci.*, 12 (2017) 11150.
27. M. Keddad, C. Kuntz, H. Takenouti, D. Schustert and D. Zuili, *Electrochim. Acta*, 42 (1997) 87.
28. A.I. Karayan, K. Jata, M. Velez and H. Castaneda, *J. Alloys Compd.*, 657 (2016) 546.
29. R. Ambat, A.J. Davenport, A. Afseth and G. Scamans, *J. Electrochem. Soc.*, 151 (2004) B53.
30. K. Nis, A. Lu, *J. Electrochem. Soc.*, 137 (1990) 69.
31. F.H. Cao, Z. Zhang, J.X. Su, Y.Y. Shi and J.Q. Zhang, *Electrochim. Acta*, 51 (2006) 1359.
32. F.N. Afshar, F.D. Tichelaar, A.M. Glenn, P. Taheri, M. Sababi, H. Terryn and J.M.C. Mol, *Corrosion*, 73 (2017) 379.
33. G.J. Marshall, R.K. Bolingbroke and A. Gray, *Met. Trans. A*, 24 (1993) 1935.
34. S. Meijers. Corrosion of aluminum brazing sheet. PhD Thesis, TU Delft (2002).
35. Y. Tu, Z. Tong and J. Jiang, *Mater. Sci. Eng. A*, 44 (2013) 1760.